Large dielectric response to the paramagnetic-ferromagnetic transition ($T_C \sim 100$ K) in multiferroic $BiMnO_3$ epitaxial thin films

Rainer Schmidt,[1,2,*] Wilma Eerenstein,[1,3] and Paul A. Midgley[1]
[1]*Department of Materials Science and Metallurgy, University of Cambridge, Pembroke Street, Cambridge CB2 3QZ, United Kingdom*
[2]*Engineering Materials, The University of Sheffield, Sir Robert Hadfield Building, Mappin Street, Sheffield S1 3JD, United Kingdom*
[3]*ECN Solar Energy, P.O. Box 1, 1755 ZG Petten, The Netherlands*
(Received 10 February 2009; published 11 June 2009)

The dielectric properties of multiferroic $BiMnO_3$ 50 nm epitaxial thin films grown on Nb-doped $SrTiO_3$ (001) substrates were analyzed by impedance spectroscopy between 55 and 155 K. One single intrinsic thin film dielectric relaxation process was deconvoluted from an extrinsic electrode interface contribution by the use of an equivalent circuit. The paramagnetic-ferromagnetic transition ($T_C \sim 100$ K) was reflected by a large peak in the thin film relative dielectric permittivity. The weak dielectric response at T_C observed previously in $BiMnO_3$ polycrystals is largely enhanced in thin films. Intrinsic noninsulating thin film resistivity below T_C was detected.

DOI: 10.1103/PhysRevB.79.214107 PACS number(s): 72.80.Ga, 75.47.Lx, 73.40.Cg

I. INTRODUCTION

The field of multiferroic materials has experienced a boom in research activity in recent years due to potential application of such materials, for example, in data storage media for dual read and write mechanisms.[1–5] In the presence of strong magnetoelectric (ME) coupling, magnetic order can be addressed by an electric field enabling independent electric writing on and magnetic reading off a multiferroic data storage bit. $BiMnO_3$ (BMO) is of particular interest for such technological aspirations due to a high magnetic moment of up to $3.6\mu_B$/Mn in bulk below the magnetic transition temperature $T_C \sim 100$ K and due to coexisting ferroelectricity.[6,7] This allows the study of fundamental aspects of multiferroic materials with strong ferromagnetism, as required for application.

The family of perovskite manganite materials has attracted great interest in the early 1990s due to colossal magnetoresistance (CMR) effects, charge and orbital ordering, and exotic phase transitions. The basis of CMR effects is phase coexistence on different length scales which arises due to strong competition of different exchange mechanisms between the *B*-site Mn cations. On the other hand, in multiferroic manganites such as BMO several order parameters can coexist simultaneously and can cooperate, for example, ferroelectricity and ferromagnetism. The ferromagnetic moment in BMO arises from the high-spin state ($S=2; t_{2g}^3 e_g^1$) of Mn^{3+} cations (identical to $LaMnO_3$) and ferromagnetic exchange interactions, which were reported to originate from orbital ordering that produces three-dimensional ferromagnetic super-exchange interaction of e_g electrons.[6] Ferroelectricity (in bulk $T_C^{FE} \sim 700$ K) originates from the displacement of Mn^{3+} cations off the centrosymmetric positions in the perovskite octahedra and the resulting dipole moment. The stabilization of both the ferromagnetism and the ferroelectric off-center distortion have been associated with the presence of Bi $6s$ lone pair electrons,[8] in contrast to $YMnO_3$, where strong rehybridization of Y $4d$ states was reported to be responsible for multiferroicity.[9] Bulk and thin film BMO properties have been reviewed in a previous publication more thoroughly.[10]

Strong ME coupling has been reported in related manganites such as $TbMnO_3$,[11] and $TbMn_2O_5$.[12] However, such materials exhibit sinusoidal, spiral, or helical spin structures representing a (canted) antiferromagnetism. It has been claimed that ferroelectric order can couple to such spiral spin structure which has been evidenced by ferroelectric polarization flops between different crystallographic directions as a result of applied magnetic fields switching the direction of the spiral spin order.[11,13] To the authors knowledge, a direct coupling of ferroelectric and ferromagnetic order has not been reported in a single phase material and it is believed that such coupling needed to be mediated by spiral spin structures or alternative mechanisms. Here in this work we present a study on thin film BMO without spiral spin structures but with a ferromagnetic parallel Mn spin alignment below $T_C \sim 100$ K of $M=2.2\mu_B$/Mn.[14]

In bulk BMO the relative dielectric permittivity shows a weak response to the magnetic transition at T_C (Fig. 1), which remarkably reduces gradually by the application of magnetic fields.[6] Here, a large peak in relative dielectric permittivity at the magnetic transition is reported across T_C in epitaxial BMO thin films. This was associated with modifications of the BMO crystal lattice at T_C representing an indirect coupling scenario via the lattice.

II. EXPERIMENTAL

Thin BMO films of 50 nm were grown epitaxially on conducting 1 at. % Nb-doped $SrTiO_3$ (STO) substrates oriented in the (001) crystal direction from Bi rich $Bi_{1.2}MnO_{3+x}$ targets, using pulsed laser deposition in flowing oxygen ambient at a pressure of 0.1 Pa. Growth, structural, magnetic, and preliminary dielectric characterizations of the films were reported previously.[10,14] Uniform strain was confirmed and narrow (002) full width at half maximum (FWHM) x-ray rocking curves of 0.04° compared to 0.03° for STO substrates were found. Films with increased thickness above 100

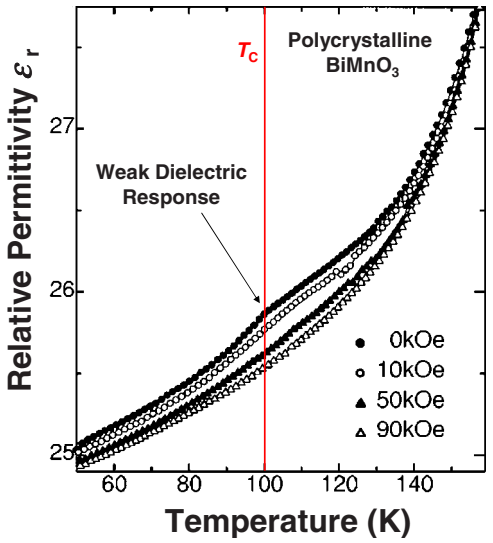

FIG. 1. (Color online) Weak dielectric response to the magnetic transition T_C in polycrystalline $BiMnO_3$, reproduced from Ref. 6: copyright of the American Physical Society (APS), reprint permitted by the APS.

nm were found to exhibit less uniform strain, i.e., strain relaxation effects. The epitaxial BMO unit cell may be indexed as pseudocubic with a small tetragonal elongation ($c/a \sim 1.015$).[15]

Pt top-top electrodes of surface area A were sputter deposited onto the film surface through a mechanical mask. The low-substrate resistivity allowed measuring the out-of-plane impedance across the film along the film normal axis using the substrate as a bottom electrode. This setup was found suitable to resolve the high electrical resistivity values of BMO at low T due to the microscopic electrode substrate distance d (i.e. film thickness). Contact to the sample electrodes was made using a custom-built impedance probe equipped with spring loaded drop-down (top-top) pins at the sample tray located near the bottom of the probe. The pins were connected to low temperature coaxial cables on the probe, which had their shielding outer conductors connected to each other close to the pins. The probe was placed in a standard vaporized He cooled cryostat (Janis) and impedance spectroscopy (IS) was carried out between 55 and 155 K in the frequency range of 40 Hz–2 MHz using an Agilent 4294A Impedance Analyzer with a signal amplitude of 50 mV.

III. IMPEDANCE SPECTROSCOPY

Impedance spectroscopy is a well-established tool to deconvolute several relaxation processes contributing to the macroscopic dielectric properties of electroceramic bulk and film samples.[16–18] Typical relaxation processes are intrinsic bulk, grain boundary, and sample electrode-interface relaxations. Such contributions can each be modeled by a resistor (R) and capacitor (C) in parallel (RC element) and the macroscopic impedance is described by an equivalent circuit containing all individual RC elements in series.[19] In BMO epitaxial multiferroic thin films, intrinsic film and extrinsic electrode-interface relaxations have been observed previously above room temperature.[10] The samples investigated in Ref. 10 have been reinvestigated in this study but at lower temperature near T_C. In Ref. 10, the interface and intrinsic film-relaxation processes had each been modeled by a nonideal RC element, where the ideal capacitor is replaced by a nonideal constant-phase element (CPE). The impedance of such a CPE is given by

$$Z^*_{\mathrm{CPE}} = \frac{1}{(i\omega)^n C}, \tag{1}$$

where the capacitance C is given in modified units of $\mathrm{F}\cdot\mathrm{s}^{n-1}$, ω is the angular frequency, and n is an empirical exponent close to 1. An ideal capacitor corresponds to $n=1$. The capacitance values obtained from a CPE can be corrected to units of Faraday/cm (F/cm) using the standard conversion.[20] Two non-ideal R-CPE elements have been employed in this study to model the film and interface relaxation in BMO epitaxial layers at low temperature (see Fig. 2). Additionally, a single series resistor was used to account for extrinsic resistance from cables and substrate and an inductor to account for the lead inductance. The full circuit has been presented and discussed in more detail previously.[10]

IV. RESULTS AND DISCUSSION

Dielectric properties of the sample were measured in terms of the real part and the imaginary part of the impedance Z' and Z''. Those values were normalized by multiplication with the geometrical factor $g(=A/2d)$, giving the specific impedance z' and z''. Complex modulus and capacitance values were obtained from the impedance using the standard conversion.[17] IS data in Fig. 2(a) were plotted on the complex plane as negative part of the specific impedance vs the real part of the specific impedance, $-z''$ vs z', whereas Fig. 2(b) shows the imaginary part of the modulus function M'' vs frequency (f) and real part of specific impedance $-z''$ vs f. Figure 2(c) shows the plot of real part of specific capacitance c' vs f. All plots reveal two relaxation processes which had been previously assigned to one single intrinsic film relaxation (R2-C2) and an extrinsic electrode sample interface (R1-C1).[10,17] Both relaxations are most clearly represented on $-z''$ vs f, M'' vs f, and c' vs f plots:[19] in Fig. 2(b) the thin film relaxation peak is clearly shown in M'' vs f (R2-C2) and the interface relaxation peak would be displayed at lower frequencies in $-z''$ vs f (R1-C1); in Fig. 2(c) the interface and thin film relaxations are separately displayed as two approximately frequency independent capacitance plateaus and the low-frequency high-capacitance plateau corresponds to the interface.[21] The lower frequency of the interface relaxation peak and the high capacitance plateau as compared to intrinsic contributions are typical features of an interface and may serve as an identification tool of its extrinsic nature.[19] Equivalent circuit fitting was performed and the fitted values were normalized to the sample geometry. The fitting results are presented in Table I. The resistivity values are shown in specific units (Ω cm), the capacitance values are shown in non-normalized CPE units, and in normalized and corrected

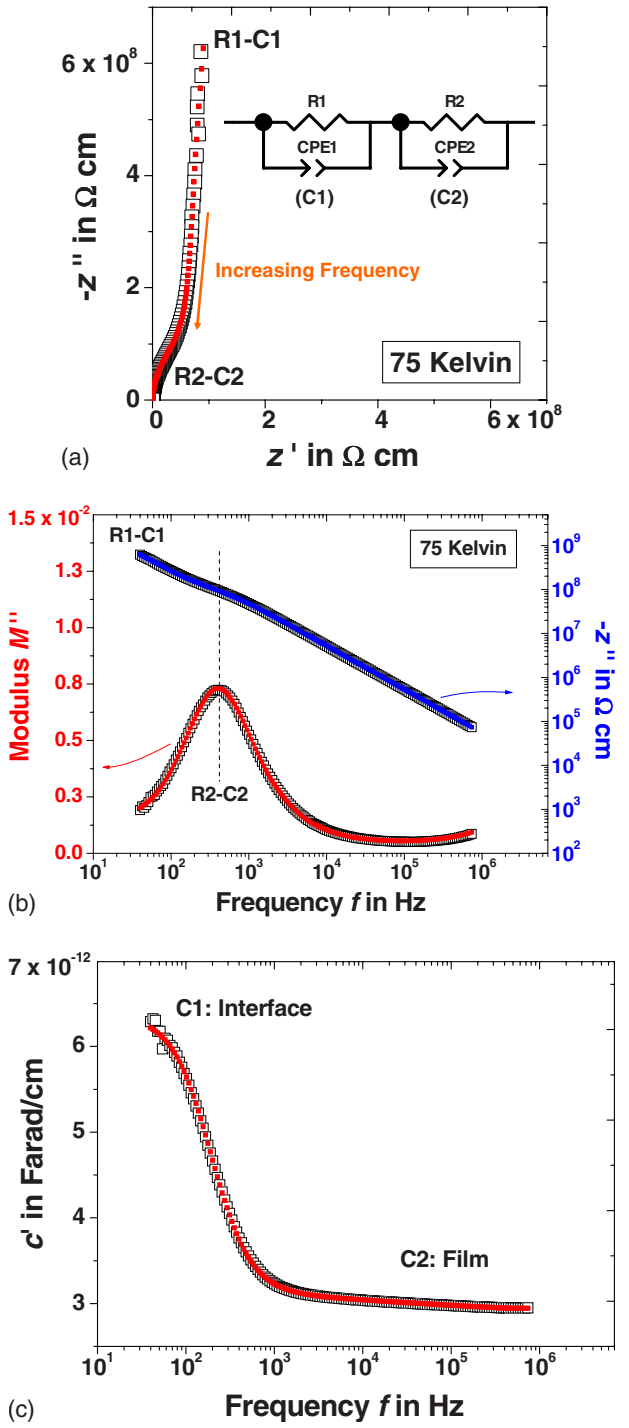

FIG. 2. (Color online) BMO 50 nm thin film IS data at 75 K plotted in different notations {data (□) and model (■)}: (a) complex specific impedance $-z''$ vs z'; (b) imaginary part of the modulus function M'' vs f, and imaginary part of the specific impedance $-z''$ vs f; and (c) real part of capacitance c' vs frequency f. Conversion between complex impedance and modulus notations was done using the standard conventions (Ref. 17). Data and model show excellent agreement.

specific capacitance units (F/cm). The CPE exponent n is dimensionless.

The film and interface resistivity trends with temperature are shown in Fig. 3, demonstrating insulating film resistivity above $T_C > 100$ K. A noninsulating film resistivity was detected below T_C, deconvoluted from all extrinsic contributions. The activation energy was determined for $T > T_C$ to be $E_A \sim 0.2$ eV, in good agreement with the high temperature value reported previously ($E_A \sim 0.23$ eV).[10,17] Such E_A value is typical for electron hopping between mixed-valence Mn cations. This may be the result of oxygen vacancies in the films ($BiMnO_{3-\delta}$), which would be compensated by reduction of some Mn^{3+} to Mn^{2+} inducing perceptible conductivity. Below T_C, the noninsulating thin film resistivity is still considerably high (Fig. 3), indicating a low concentration of charge carriers and oxygen vacancies. The transition from insulating to noninsulating film resistivity may be explained by the onset of weak double-exchange interactions between Mn valence d electrons, which is commonly observed in ferromagnetic manganite perovskites below T_C. The extrinsic interface resistance is larger than the intrinsic film resistance which implies that the dc resistance is dominated by the interface. Therefore, dc or limited frequency range measurements may be unreliable to assess the film leakage behavior.

Large response of both the intrinsic dielectric thin film and extrinsic interface capacitance to the paramagnetic-ferromagnetic (PM-FM) transition at T_C are shown in Figs. 4(a) and 4(b). Capacitance values obtained from a CPE were converted into real capacitances,[20] which were then converted into the relative dielectric permittivity ε_r in case of the film contribution.

The peak structure in the plot of thin film relative dielectric permittivity ε_r vs T shows that ε_r increases by a factor of ~ 3 at T_C, although no ferroelectric transition is expected. In polycrystalline BMO only a weak dielectric anomaly had been reported at T_C (Fig. 1).[6] Therefore, the strong peak observed here may arise due to the epitaxial nature of the films, i.e., high crystalline orientation and/or epitaxial strain, which is absent in polycrystals. Generally, the relative dielectric permittivity ε_r values reported here are lower in magnitude compared to room temperature measurements.[10] This is consistent with the strongly temperature dependent dielectric permittivity in BMO reported previously.[6] This ε_r increase with increasing temperature may be a manifestation of the film ferroelectric transition at $T_C(\mathrm{FE}) \sim 450$ K (Ref. 22) since a continuous increase in ε_r is expected at $T < T_C(\mathrm{FE})$.

Such a large peak in ε_r at zero applied magnetic fields has been observed in multiferroic oxides with an antiferromagnetic spiral or helical spin structure at the transition from a noncollinear to collinear spin-density wave periodicity (or noncommensurate to commensurate transition)[11] but not at a PM-FM transition. The possibility of a large direct ME coupling effect in BMO thin films may not be plausible in the absence of spiral or helical spin structure. Parallel ferromagnetic spins are unlikely to strongly couple directly to the ferroelectric order. The origin of this large dielectric response may be better explained by an indirect coupling via the lattice due to a crystal structure transition of thin film $BiMnO_3$ at the magnetic phase transition. $BaTiO_3$ is a prominent example where a crystal structure transition within a ferroelectric phase results in a peak structure in the relative dielectric permittivity vs temperature curves.[23]

TABLE I. Equivalent circuit-fitting values; capacitance values are given in modified CPE units of $F \cdot s^{n-1}$ (non-normalized), and in corrected and normalized units specific capacitance F/cm. The CPE exponent n [Eq. (1)] is dimensionless.

Temperature K	Resistivity R1 (Ωcm)	Capacitance C1 (CPE)	CPE1 exp. n	Specific C C1 (F/cm)	Resistivity R2 (Ωcm)	Capacitance C2 (CPE)	CPE1 exp. n	Specific C C2 (F/cm)
55.83	2.06×10^{10}	6.19×10^{-12}	1.00	6.19×10^{-7}	7.01×10^{7}	6.69×10^{-12}	0.99	5.98×10^{-12}
65.65	2.00×10^{10}	6.28×10^{-12}	1.00	6.28×10^{-7}	8.56×10^{7}	6.82×10^{-12}	0.98	6.08×10^{-12}
75.72	1.61×10^{10}	6.41×10^{-12}	1.00	6.41×10^{-7}	6.71×10^{7}	6.95×10^{-12}	0.98	6.10×10^{-12}
85.86		6.68×10^{-12}	1.00	6.68×10^{-7}	1.20×10^{8}	6.81×10^{-12}	0.98	6.08×10^{-12}
95.95	4.46×10^{9}	5.28×10^{-12}	0.99	5.15×10^{-7}	2.42×10^{8}	1.17×10^{-11}	0.97	9.99×10^{-12}
101.05	3.24×10^{9}	4.44×10^{-12}	0.99	4.26×10^{-7}	6.93×10^{7}	2.35×10^{-11}	0.96	1.86×10^{-11}
106.15	2.16×10^{9}	5.10×10^{-12}	0.99	4.86×10^{-7}	8.49×10^{7}	1.68×10^{-11}	0.96	1.31×10^{-11}
116.32	9.51×10^{8}	9.16×10^{-12}	0.98	8.51×10^{-7}	1.09×10^{8}	9.36×10^{-12}	0.96	7.04×10^{-12}
126.48	5.85×10^{8}	2.08×10^{-11}	0.96	1.69×10^{-6}	5.45×10^{7}	8.60×10^{-12}	0.95	5.91×10^{-12}
136.6		4.51×10^{-11}	0.90	3.17×10^{-6}	1.77×10^{7}	9.71×10^{-12}	0.95	6.11×10^{-12}
146.61		6.06×10^{-11}	0.89	3.81×10^{-5}	5.53×10^{6}	1.28×10^{-11}	0.93	6.28×10^{-12}
156.7		5.20×10^{-11}	0.93	3.87×10^{-5}	2.05×10^{6}	1.99×10^{-11}	0.90	6.34×10^{-12}

An alternative explanation for the peak in ε_r vs T as a result of a phase transition in the Nb-STO substrate could be excluded. Undoped STO is known to enter into an antiferrodistortive phase by cooling below the transition temperature of ~100 K,[24] which is associated with slight rotations of the TiO_6 octahedra.[25] The STO antiferrodistortive transition temperature would match well with T_C in $BiMnO_3$. However, an undoped STO wafer substrate was investigated and showed no response of the wafer relative dielectric permittivity to the antiferrodistortive transition at ~100 K [Fig. 4(c)]. The antiferrodistortive transition in the STO wafer is uncoupled from the dielectric properties. Small Nb doping of STO may be unlikely to strongly modify or enhance the antiferrodistortive phase and the Nb-STO substrate is expected to show no significant dielectric response to a potential antiferrodistortive phase transition. Therefore, the ferrodistortive transition in STO may not be the origin of the large dielectric response effect reported here in BMO/Nb-STO thin film structures.

However, this issue certainly points toward the interesting possibility to include an additional "ferroic" property into a multiferroic epitaxial layer assemblage by the choice of an antiferrodistortive or ferroelastic substrate. The film-substrate structure investigated here may well be truly "multiferroic" below T_C in the ferromagnetic, ferroelectric (BMO), and antiferrodistortive (STO) state.

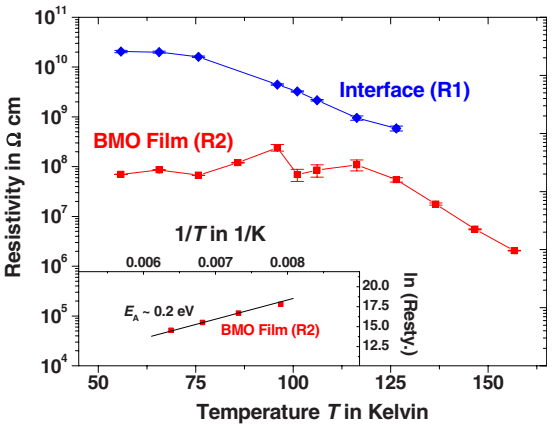

FIG. 3. (Color online) BMO thin film resistivity R2 (■) and interface R1 (♦) plotted as ρ vs T; Inset: $\ln(\rho)$ vs $1/T$ at 125–155 K giving a thin-film activation energy $E_A \sim 0.2$ eV.

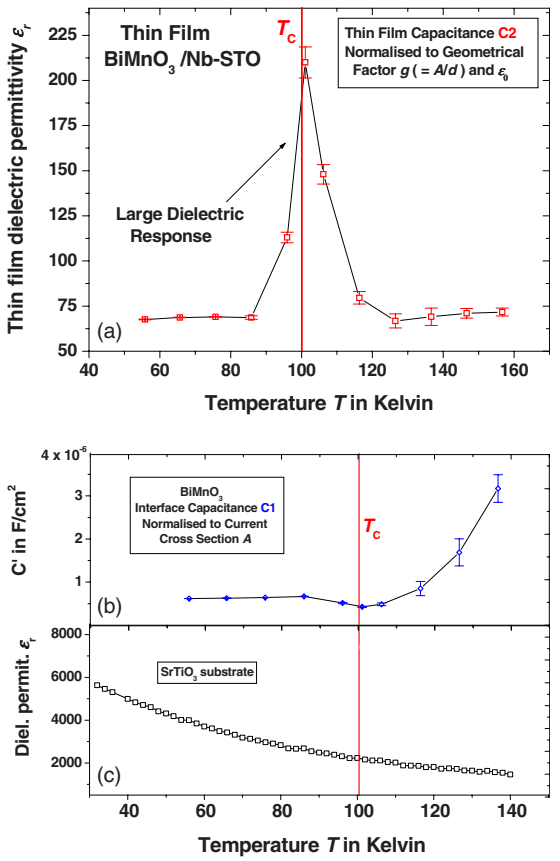

FIG. 4. (a) (Color online) BMO film capacitance C2 (□) plotted as relative dielectric permittivity ε_r vs T; (b) BMO interface capacitance C1 (◇) normalized to current cross section A; (c) intrinsic $SrTiO_3$ relative dielectric permittivity (□).

V. CONCLUSIONS

The BMO epitaxial layers investigated showed a noninsulating film resistivity below T_C probably due to the onset of double-exchange interactions below T_C. The intrinsic thin-film BMO dielectric response at T_C is largely amplified in epitaxial thin films as compared to polycrystals. Such difference may therefore be ascribed to high crystalline order and/or epitaxial strain in the films. Large dielectric response at T_C may be associated most likely with structural changes in the BMO crystal structure. The large peak in the intrinsic BMO film dielectric permittivity at the magnetic transition suggests an indirect coupling effect via the lattice. Extrinsic contributions were deconvoluted.

ACKNOWLEDGMENTS

The authors wish to thank Finlay Morrison, Ian Reaney, and Jan Pokorny for useful discussions. R.S. wishes to acknowledge financial support from the Leverhulme Trust. W.E. is grateful to the EU.

*Corresponding author; rainerxschmidt@googlemail.com

[1] M. Fiebig, J. Phys. D **38**, R123 (2005).
[2] W. Eerenstein, N. D. Mathur, and J. F. Scott, Nature (London) **442**, 759 (2006).
[3] N. A. Spaldin and M. Fiebig, Science **309**, 391 (2005).
[4] S. W. Cheong and M. Mostovoy, Nature Mater. **6**, 13 (2007).
[5] R. Ramesh and N. A. Spaldin, Nature Mater. **6**, 21 (2007).
[6] T. Kimura, S. Kawamoto, I. Yamada, M. Azuma, M. Takano, and Y. Tokura, Phys. Rev. B **67**, 180401(R) (2003).
[7] H. Chiba, T. Atou, and Y. Syono, J. Solid State Chem. **132**, 139 (1997).
[8] R. Seshadri and N. A. Hill, Chem. Mater. **13**, 2892 (2001).
[9] D.-Y. Cho, J.-Y. Kim, B.-G. Park, K.-J. Rho, J.-H. Park, H.-J. Noh, B. J. Kim, S.-J. Oh, H.-M. Park, J.-S. Ahn, H. Ishibashi, S.-W. Cheong, J. H. Lee, P. Murugavel, T. W. Noh, A. Tanaka, and, T. Jo, Phys. Rev. Lett. **98**, 217601 (2007).
[10] R. Schmidt, W. Eerenstein, T. Winiecki, F. D. Morrison, and P. A. Midgley, Phys. Rev. B **75**, 245111 (2007).
[11] T. Kimura, T. Goto, H. Shintani, K. Ishizaka, T. Arima, and Y. Tokura, Nature (London) **426**, 55 (2003).
[12] N. Hur, S. Park, P. A. Sharma, J. S. Ahn, S. Guha, and S. W. Cheong, Nature (London) **429**, 392 (2004).
[13] Y. Yamasaki, S. Miyasaka, T. Goto, H. Sagayama, T. Arima, and Y. Tokura, Phys. Rev. B **76**, 184418 (2007).
[14] W. Eerenstein, F. D. Morrison, J. F. Scott, and N. D. Mathur, Appl. Phys. Lett. **87**, 101906 (2005).
[15] C.-H. Yang, T. Y. Koo, S.-H. Lee, C. Song, K.-B. Lee, and Y. H. Jeong, Europhys. Lett. **74**, 348 (2006).
[16] *Impedance Spectroscopy*, edited by J. R. Macdonald (John Wiley & Sons, New York, 1987).
[17] R. Schmidt, in *Ceramic Materials Research Trends*, edited by P. B. Lin (Nova Science Publishers, Hauppauge, NY, 2007), p. 321.
[18] R. Schmidt, J. Wu, C. Leighton, and I. Terry, Phys. Rev. B **79**, 125105 (2009).
[19] J. T. S. Irvine, D. C. Sinclair, and A. R. West, Adv. Mater. **2**, 132 (1990).
[20] C. H. Hsu and F. Mansfeld, Corrosion **57**, 747 (2001).
[21] G.-Z. Liu, C. Wang, C.-C. Wang, J. Qiu, M. He, J. Xing, K.-J. Jin, H.-B. Lu, and G.-Z. Yang, Appl. Phys. Lett. **92**, 122903 (2008).
[22] A. Moreira dos Santos, S. Parashar, A. R. Raju, Y. S. Zhao, A. K. Cheetham, and C. N. R. Rao, Solid State Commun. **122**, 49 (2002).
[23] A. von Hippel, Rev. Mod. Phys. **22**, 221 (1950).
[24] S. Ravy, D. Le Bolloch, R. Currat, A. Fluorasu, C. Mocuta, and B. Dkhil, Phys. Rev. Lett. **98**, 105501 (2007).
[25] H. Unoki and T. Sakudo, J. Phys. Soc. Jpn. **23**, 546 (1967).